Available online at www.sciencedirect.com
SCIENCE DIRECT
Polymer 47 (2006) 3494–3504
polymer
www.elsevier.com/locate/polymer

Oriented and exfoliated single wall carbon nanotubes in polyacrylonitrile

Han Gi Chae, Marilyn L. Minus, Satish Kumar *,[1]

School of Polymer, Textile and Fiber Engineering, Georgia Institute of Technology, P.O. Box 0295, Atlanta, GA 30332-0295, USA

Received 7 February 2006; received in revised form 13 March 2006; accepted 14 March 2006
Available online 3 April 2006

Abstract

Polyacrylonitrile (PAN)/single wall carbon nanotubes (SWNT) fibers were gel spun at 0, 0.5, and 1 wt% SWNT content to a draw ratio of 51. Structure, morphology, and mechanical and dynamic mechanical properties of these fibers have been studied. PAN/SWNT composite exhibited much higher electron beam radiation resistance than PAN. As a result, PAN lattice images could be easily observed in the composite fiber by high resolution transmission electron microscopy. The PAN/SWNT composite fiber also exhibited higher solvent resistance than the control PAN fiber. UV–vis spectroscopy of highly drawn fiber exhibited van Hove transitions, suggesting SWNT exfoliation upon drawing. SWNT exfoliation was also confirmed by high resolution transmission electron microscopy (HRTEM). At 1 wt% SWNT loading, fiber storage modulus (at 1 Hz) increased by 13.9, 6.6, and 0.2 GPa at −75, 25, and 150 °C, respectively. This suggests that the load transfer ability and hence interfacial strength is increasing with decreasing temperature, even below the polymer's γ transition temperature.

Keywords: Polyacrylonitrile; Single wall carbon nanotube; Gel spinning

1. Introduction

Polymer/carbon nanotube (CNT) composite films and fibers are of significant current interest [1]. While, numerous polymer/CNT composite systems have been processed with significantly improved properties [2–10], SWNT exfoliation and orientation in polymer matrices remains a challenge. The orientation requirement for achieving high modulus in CNT based fibers [11] is similar to that for achieving high modulus in polymeric and carbon fibers. Ultra high orientation and hence high modulus in polymeric fibers such as Kevlar™, Zylon™, and pitch based carbon fibers [12] is achieved by spinning from liquid crystalline media. Modulus value as high as 827 GPa (>78% of the theoretical value for graphite) has been achieved in commercial pitch based carbon fiber (P120) [13]. Ultra high orientation in polymers can also be achieved by gel spinning. Gel spun polyethylene fiber was commercialized in 1980s [14,15]. Gel spinning has also been demonstrated on poly(vinyl alcohol) (PVA) [16,17] and PAN [18–23]. Recently, PAN/CNT composites have attracted significant attention [8,24–37]. In this study, PAN/SWNT composite fiber was gel spun, demonstrating good SWNT orientation and exfoliation. Structure and properties of the fiber have been studied and compared to the properties of the control gel spun PAN fiber.

2. Experimental

PAN (viscosity average molecular weight $= 2.5 \times 10^5$ g/mol) was obtained from Exlan, Co. (Japan). Purified SWNTs were obtained from Carbon Nanotechnologies, Inc. (Houston, TX). Based on thermogravimetric analysis (TGA) in air, SWNTs used in this study contain less than 1 wt% metallic impurity. The bright field transmission electron micrograph (Fig. 1) shows SWNT bundle diameter as large as 100 nm. Dimethyl formamide (DMF) from Sigma–Aldrich, Co. was used as received. SWNTs were dispersed in DMF at a concentration of 40 mg/L using 24 h bath sonication (Branson 3510R-MT, 100 W, 42 kHz) at room temperature. PAN (15 g) was dried in vacuum at 100 °C and dissolved in DMF (100 mL) at 80 °C. Optically homogeneous SWNT/DMF dispersion was added to the PAN/DMF solution. The excess amount of solvent was evaporated by vacuum distillation at 80 °C, while stirring, to obtain the desired solution concentration (15 g solids (PAN + SWNT)/100 mL solvent). Similarly, other solutions were prepared to yield SWNT concentration with respect to the polymer of 0, 0.5, and 1 wt%. The PAN/DMF and PAN/SWNT/DMF solutions were spun at 31.4 m/min using a 500 μm diameter single hole spinneret at 110 °C into a methanol

* Corresponding author. Tel.: +1 404 894 7550; fax: +1 404 894 8780.
E-mail addresses: hangi.chae@gatech.edu (H.G. Chae), marilyn.minus@ptfe.gatech.edu (M.L. Minus), satish.kumar@gatech.edu (S. Kumar).
[1] http://www.ptfe.gatech.edu/faculty/kumar/kumar.html.

0032-3861/$ - see front matter © 2006 Elsevier Ltd. All rights reserved.
doi:10.1016/j.polymer.2006.03.050

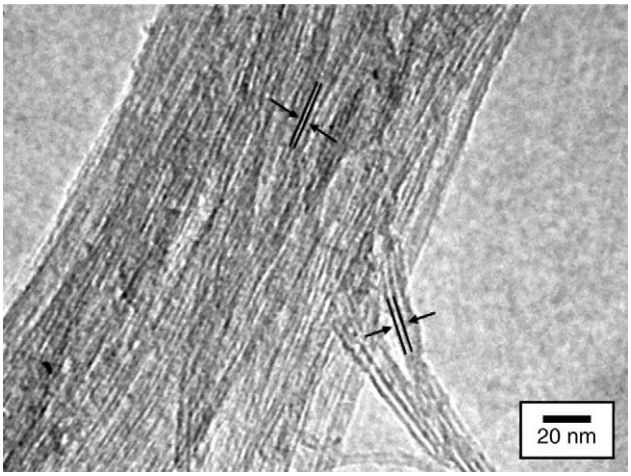

Fig. 1. Bright field TEM image of SWNT used in this study.

bath maintained at −50 °C. The air gap between spinneret and the methanol bath was about 2 cm. The as-spun fibers were taken up at 100 m/min and were kept immersed in methanol bath (maintained between −20 and −40 °C) for 1 week, to ensure gelation. As a result, the as spun fiber draw ratio was 3.2. The gel fiber was further drawn (draw ratio in the range of 7–16) at 160 °C in glycerol bath followed by washing in ethanol and vacuum drying at 40 °C for 3 days. The total draw ratio, determined by multiplying spin draw ratio with post draw ratio, was as high as 51.

Optical microscopy was carried out using a Leitz polarizing microscope. UV–vis spectra on solution and various fibers were obtained using SEE 1100 microspectrometer. Single filament tensile properties were determined using RSA III solids analyzer (Rheometric Scientific, Co.) at a gauge length of 25 mm and the crosshead speed of 0.25 mm/s. For each sample, 15 filaments were tested. Dynamic mechanical tests were also conducted using RSA III at 0.1, 1, and 10 Hz at a heating rate of 1 °C/min on a bundle of 10 filaments, also using a gauge length of 25 mm. Raman spectra were collected in the back scattering geometry using Holoprobe Research 785 Raman Microscope made by Kaiser Optical System using 785 nm excitation laser with polarizer and analyzer parallel to each other (vv mode). Spectra were obtained with the fiber axis at 0, 5, 10, 20, 30, 40, 50, 60, 70, 80, 85, and 90° from the polarization direction. The SWNT orientation in the composite fiber was determined from the peak intensity of the tangential band (ca. 1590 cm^{-1}) at various polarization angles. WAXD patterns were obtained on multifilament bundles on Rigaku Micromax-007 ($\lambda = 1.5418$ Å) using Rigaku *R*-axis IV++ detection system. The diffraction patterns were analyzed using AreaMax V. 1.00 and MDI Jade 6.1. From the azimuthal scans of the diffraction peak at $2\theta \sim 17°$, PAN molecular orientation was determined [8,38]. The crystallinity was determined using the integrated scans and the areas of the deconvoluted peaks. For baseline subtraction, linear line was drawn between $2\theta =$ 10 and 50°. The PAN crystal size was also determined from the

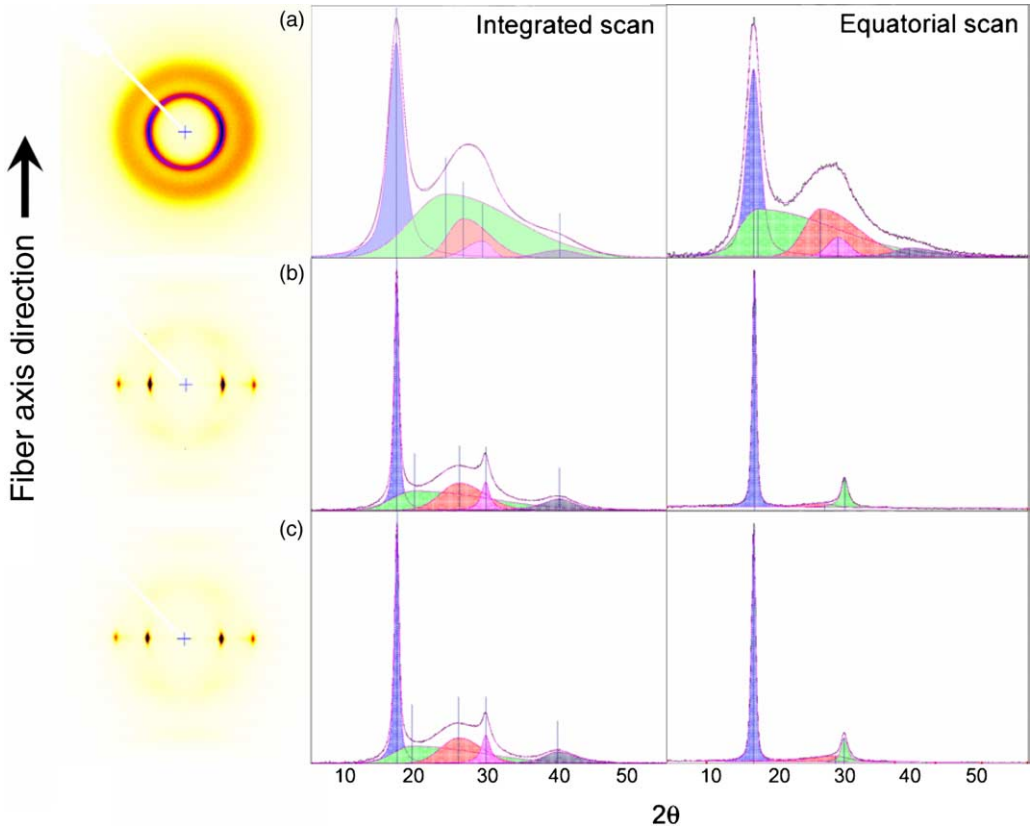

Fig. 2. WAXD photographs and deconvoluted integrated and equatorial scans. (a) PAN draw ratio 3.2, (b) PAN draw ratio 51, and (c) PAN/SWNT (1 wt%) draw ratio 51.

Table 1
WAXD results for gel-spun PAN and PAN/SWNT composite fibers

	Control PAN (draw ratio)				PAN/SWNT (0.5 wt%, DR=51)	PAN/SWNT (1 wt%, DR=51)
	3.2	22	32	51		
Crystallinity (%)	47	59	64	65	68	69
f[a]	0.13	0.90	0.91	0.92	0.92	0.93
Crystallite size (nm)	3.2	10.4	11.3	11.7	11.2	11.5
Meridional peak position (2θ, degrees)	40.2	39.9	39.9	39.7	39.5	39.4

[a] f=Herman's orientation factor, DR=draw ratio.

equatorial peak at $2\theta\sim17°$ using Scherrer equation ($K=0.9$). Fiber tensile fracture surfaces were observed on the gold coated samples by scanning electron microscopy (LEO 1530 SEM operated at 18 kV). Transmission electron microscopy study was conducted using Hitachi HF-2000 (operated at 200 kV). For TEM specimen preparation, the PAN/SWNT composite fiber (draw ratio 51) containing 1 wt% SWNT was heated in DMF at 150 °C for 30 min. The disintegrated fibrils were collected on lacey carbon TEM grids. TEM beam alignment and stigmation corrections were performed using evaporated aluminum standard (cat# 80044, EMS, Co.).

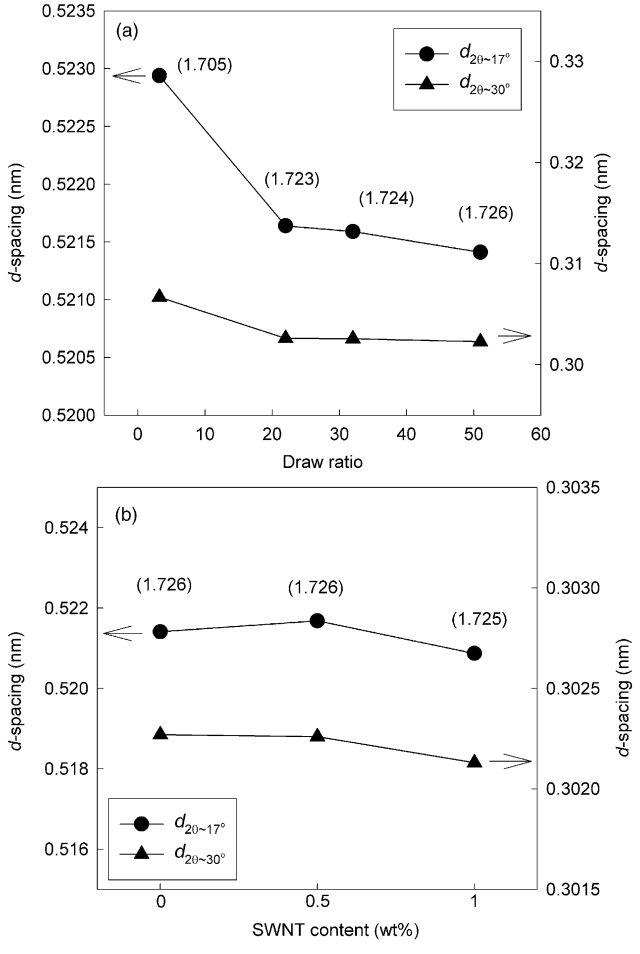

Fig. 3. Change in equatorial PAN d-spacings (for $2\theta\sim17$ and 30° diffraction peaks). (a) PAN as a function of draw ratio and (b) PAN/SWNT composite as a function of SWNT content at 51 draw ratio. The values in parenthesis are the ratios of the two d-spacings.

3. Results and discussion

Crystal structure of PAN is reported to be either hexagonal or pseudo-hexagonal with two-dimensional order [39,40], or orthorhombic with three dimensional order [41,42]. In a review of PAN crystal structure, Bashir [43] reported that the orthorhombic crystal form is due to the co-crystallization of PAN with polar solvents such as propylene carbonate and ethylene carbonate, etc. and that hexagonal crystal can be formed upon removing these solvent molecules. WAXD photographs, as well as integrated and equatorial 2θ scans for PAN and PAN/SWNT (1 wt%) fibers are given in Fig. 2. Various structural parameters determined from the X-ray study for the control PAN fiber at several draw ratios and for the fully drawn composite fibers are listed in Table 1. The equatorial peaks at $2\theta\sim17$ and 30° shift to higher angles with increasing draw ratio (Fig. 3(a)), resulting in closer packing as the transverse dimension of the PAN molecules decreases with stretching (Fig. 4). The equatorial d-spacing of the fully drawn fiber further decreased with the incorporation of SWNT (Fig. 3(b)). The ratio of these two equatorial d-spacings (Fig. 3(a)) for the as spun PAN sample (1.705) is significantly less than the value for hexagonal packing, which is $\sqrt{3}=1.732$. On drawing, this ratio approaches the hexagonal packing value of 1.732, both in the control PAN as well as in PAN/SWNT composite. The decrease in d-spacing for the control gel spun

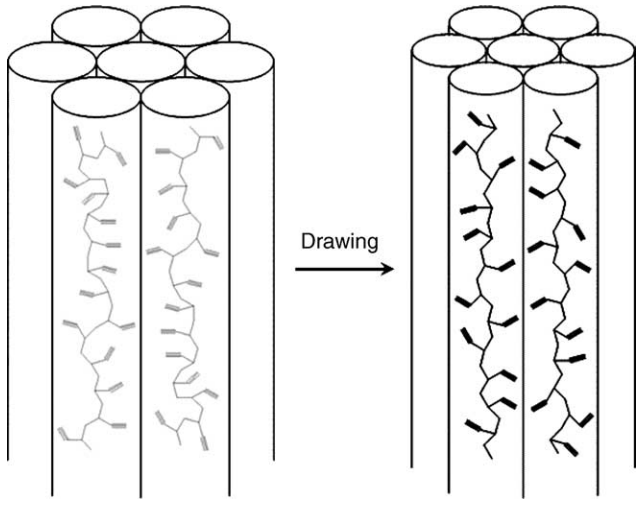

Fig. 4. Schematic of the PAN hexagonal crystal (adapted from Ref. [44]).

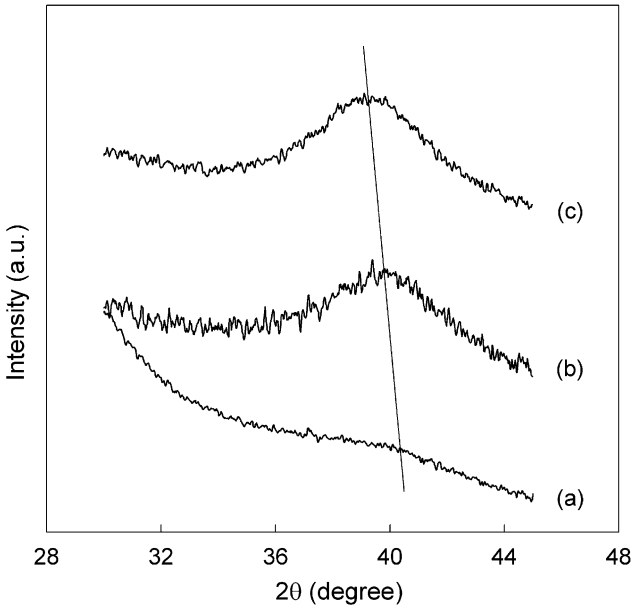

Fig. 5. WAXD meridional scans. (a) PAN draw ratio 3.2, (b) PAN draw ratio 51, and (c) PAN/SWNT (1 wt% SWNT) draw ratio 51.

PAN as a function of draw ratio is consistent with the literature reports [21,43,44].

With increasing draw ratio, planar zigzag sequences are likely to increase while the helical sequences in the crystal will be decreased. This conformational difference can be seen from the meridional peak. Generally PAN meridional peak can be deconvoluted into two peaks at $2\theta \sim 36$ and 40° resulting from the planar zigzag and helical sequences, respectively [21]. The control PAN and the PAN/SWNT composite in this study do not reveal two peaks (Fig. 5). However, the peak position is shifted to lower angle with increasing draw ratio as well as with the incorporation of SWNT (Table 1), suggesting tendency for increasing planar zigzag sequences. Crystallinity, orientation, and crystal size increase with increasing draw ratio. Composite fibers exhibited slightly higher crystallinity, polymer orientation, and somewhat lower crystal size when compared to the control fiber of the same draw ratio (draw ratio 51).

Scanning electron micrographs of the tensile fractured fiber surfaces show that both the control and composite fibers exhibit fibrillar structure. Pulled out nanotubes can also be seen in the composite fiber (Fig. 6). Bright field high resolution transmission electron micrographs of PAN/SWNT (1 wt%) fiber show aligned and exfoliated SWNTs (Fig. 7(a) and (b)). PAN crystal lattice (0.52 nm spacing) can also be

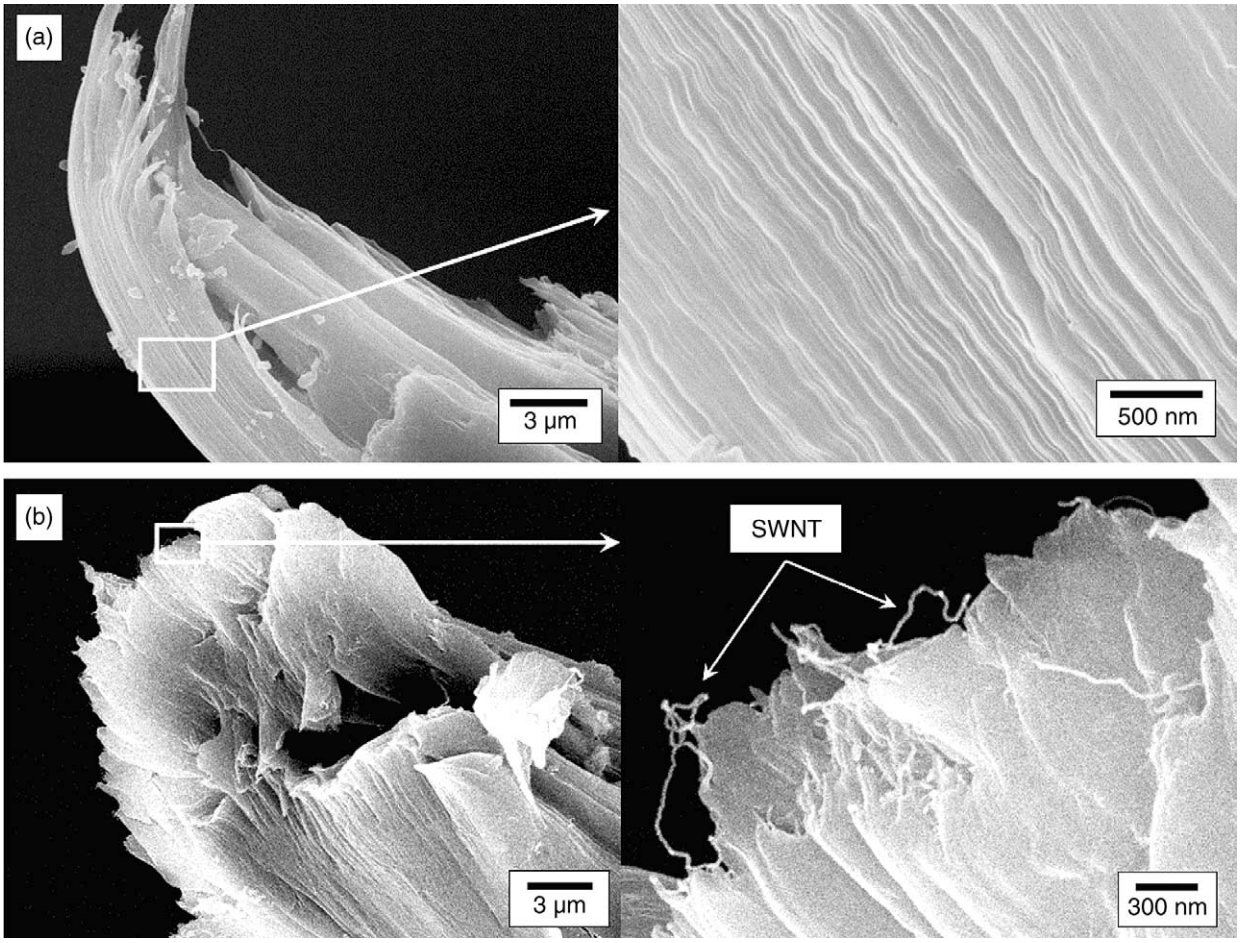

Fig. 6. Scanning electron micrographs for the fractured surface of (a) PAN fiber and (b) PAN/SWNT (1 wt%) fibers. Draw ratio of both fibers is 51.

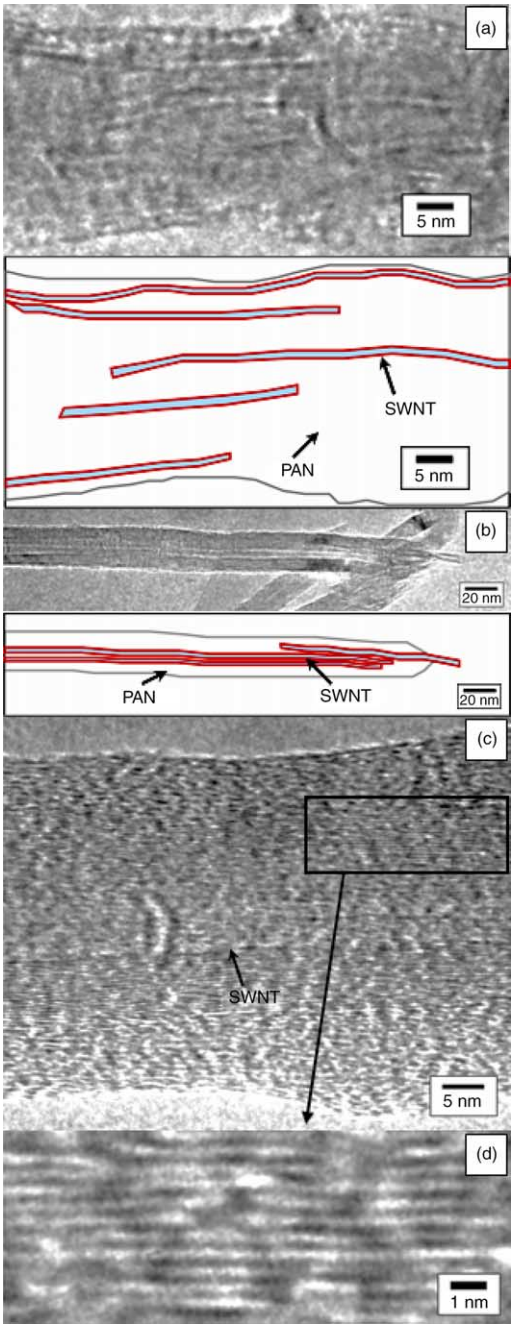

Fig. 7. (a) and (b) HRTEM images and their schematics of PAN/SWNT (1 wt%) fiber of draw ratio 51 (c) and (d) HRTEM lattice images of the same fiber.

observed in the SWNT vicinity (Fig. 7(c) and (d)). Pulled out SWNTs observed in Fig. 6 are in fact thought to be PAN covered SWNTs as seen in HRTEM images in Fig. 7. It is noted that the PAN/SWNT composites are highly resistant to the electron beam providing ample opportunity for high resolution TEM imaging. By comparison, control PAN fiber was significantly more radiation sensitive and could not be lattice imaged under the comparable imaging conditions. During TEM imaging, PVA/SWNT was also observed to exhibit much higher electron beam resistance than the control PVA [45]. These observations suggest that polymer/

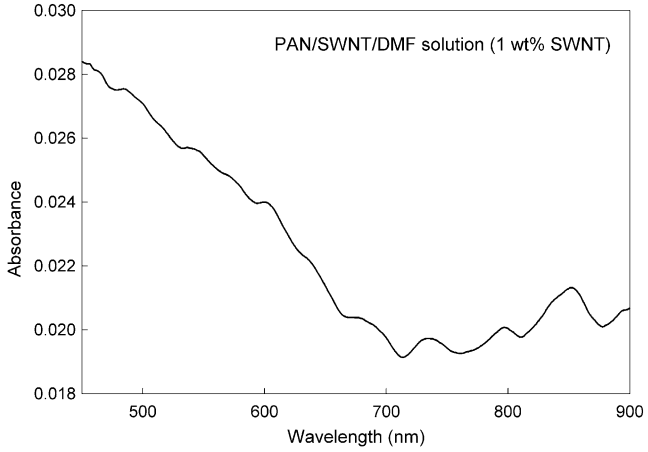

Fig. 8. UV–vis spectrum for PAN/SWNTs/DMF solution (SWNT content is 1 wt% with respect to the polymer).

SWNT crystals may in general be easier to image in the electron beam than the polymer alone.

Exfoliated SWNTs exhibit van Hove transitions, while these transitions are suppressed in SWNT bundles. The transitions are also not observed in SWNTs doped with electron donor or acceptor. The dilute PAN/SWNT/DMF solution before DMF evaporation showed van Hove transitions, suggesting SWNT exfoliation in solution (Fig. 8). However, the as spun gel fiber did not exhibit van Hove transitions (Fig. 9(a)), suggesting SWNT re-aggregation during processing. The composite fiber with the intermediate draw ratio of 32 also did not exhibit these transitions. However, the fully drawn composite fiber (draw ratio 51) exhibited van Hove transitions, suggesting that SWNT exfoliation occurred during drawing (Fig. 9(c)). The schematic of the SWNT exfoliation process is also shown in Fig. 9.

The G-band intensity ratio, with polarization parallel and perpendicular to the fiber axis, at about 1592 cm^{-1} is taken as a measure of SWNT orientation in composite [46–48] and in SWNT fibers [49]. The full width at half maximum intensity (FWHM) from WAXD azimuthal scan of SWNT (1,0) plane has also been used to measure the SWNT orientation in fibers [49–54]. Fig. 10(a) shows the G-band Raman spectra when the angle between polarizer and fiber axis are 0 and 90°, and gives the Raman G-band ratio for the PAN/SWNTs composite fiber (1 wt% SWNT, draw ratio 51) of 42. For comparison, the Raman G-band ratio for the SWNT fiber processed from liquid crystalline SWNT/H_2SO_4 solution [49] was 20.

Raman intensity as a function of SWNT orientation can be given by the following equation [55,56]

$$I^{VV}_{Fiber}(\Phi) \propto \left(\cos^4\Phi - \frac{6}{7}\cos^2\Phi + \frac{3}{35}\right)\langle P_4(\cos\theta)\rangle + \left(\frac{6}{7}\cos^2\Phi - \frac{2}{7}\right)\langle P_2(\cos\theta)\rangle + \frac{1}{5}$$

where

$$\langle P_2 \cos\theta\rangle = \frac{3\langle\cos^2\theta\rangle - 1}{2}$$

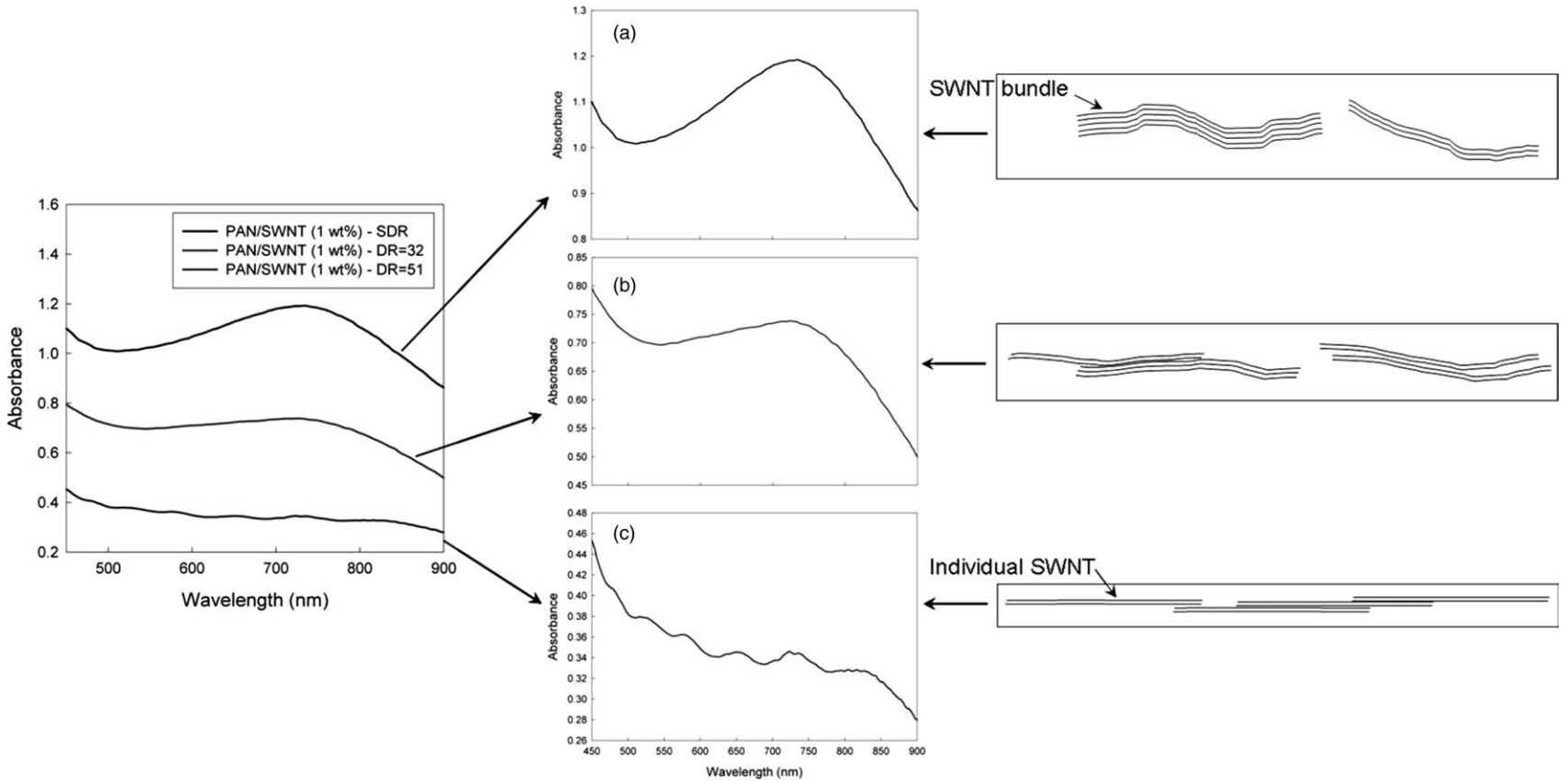

Fig. 9. UV–vis spectra and the schematics of carbon nanotubes in PAN/SWNT (1 wt%) fiber at various draw ratios as follows: (a) 3.2, (b) 32, and (c) 51.

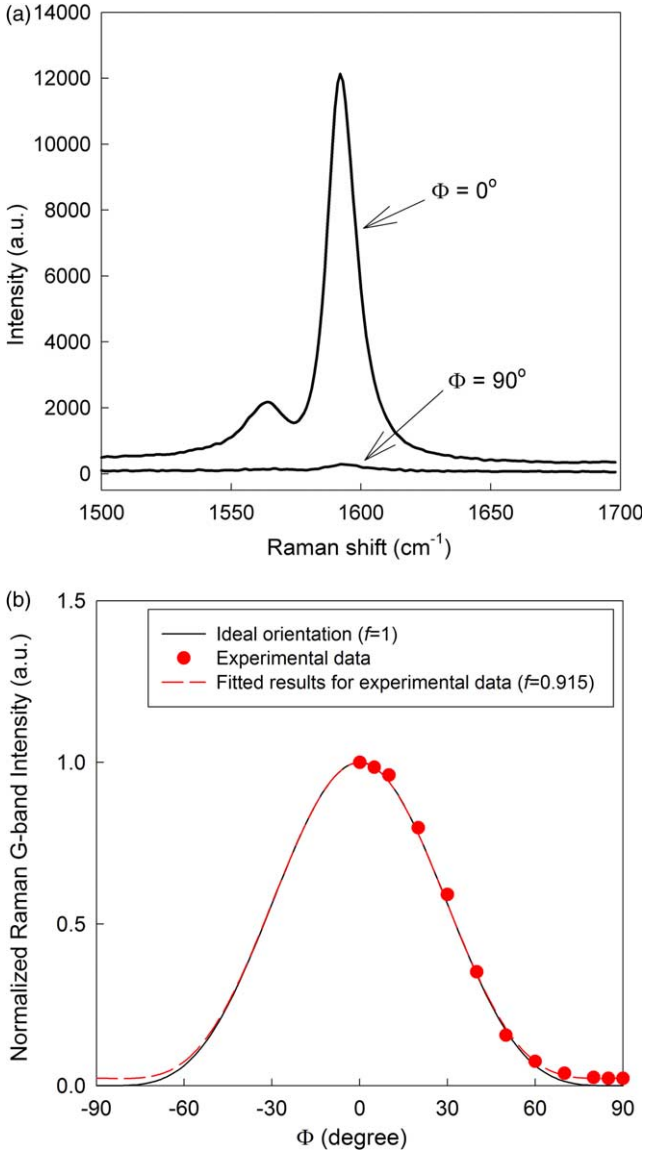

Fig. 10. (a) G-band Raman spectra for PAN/SWNT (1 wt%) fiber of draw ratio 51. The angle between polarizer and the fiber axis are 0 and 90°. (b) The normalized Raman G-band intensity distribution as a function of angle between polarizer and the fiber axis. Circles represent the experimental data for PAN/SWNT (1 wt%) fiber of draw ratio 51.

and

$$\langle P_4(\cos\theta)\rangle = \frac{35\langle\cos^4\theta\rangle - 30\langle\cos^2\theta\rangle + 3}{8}$$

and Φ and θ are the angles between the polarizer and composite fiber axis, and between SWNT axis and the composite fiber axis, respectively. The second order orientation parameter, $\langle P_2(\cos\theta)\rangle$, is the Herman's orientation factor, f. From the experimental Raman intensity data plotted in Fig. 10(b), SWNT Herman's orientation factor, f, was calculated to be 0.915, while the fourth order orientation parameter, $\langle P_4(\cos\theta)\rangle$, was calculated to be 0.96 for the fully drawn PAN/SWNT (1 wt%) fiber using the least square fit of the above equation. These orientation values were determined without assuming any particular peak shape for the Raman intensity distribution as a function of polarization angle. For comparison it should be noted that PAN/SWNT fibers spun by conventional solution spinning reported by us earlier [24], SWNT Herman's orientation factor was calculated to be 0.98 assuming Gaussian Raman intensity distribution. Re-examination of the raw data from this study showed that, when no particular peak shape was assumed (a method used in the current study), an orientation factor of 0.90 was obtained for the conventional spun PAN/SWNT fiber. Raman intensity ratio for the beam polarized parallel and perpendicular to the fiber axis was 38 for this conventional spun sample as compared to 42 for the gel spun sample. Thus the SWNT orientation in the gel spun fiber is only slightly higher (0.915) than in the conventional spun fiber (0.90). However, the SWNT orientation in the PAN/SWNT gel spun fiber is less than polymer orientation achieved in fibers such as Kevlar™, Zylon™, and Spectra™, where typical orientation factor value is ~0.99.

It was previously reported that the PAN fiber processed by conventional solution spinning was soluble in DMF at room temperature, while PAN/SWNT fiber containing 10% SWNTs was not soluble [8]. In the current study, we observed that fully drawn gel spun PAN fiber as well as PAN/SWNT (1 wt%) are both insoluble in DMF at room temperature. Drawn gel spun PAN did dissolve when boiled in DMF, while the drawn PAN/SWNT (1 wt%) only broke into fragments after boiling in DMF for 30 min. These fragments when observed in HRTEM, showed highly crystalline PAN well adhered to SWNTs (Fig. 7(c)). To show the solubility difference, PAN and PAN/SWNT fibers were heated in DMF at 60 °C for 6 h. Under these conditions, control gel spun PAN fiber begins to disintegrate into fibrils, while the 1 wt% SWNT containing composite fiber did not (Fig. 11). TEM observation that PAN crystals are well adhered to SWNTs, and X-ray result showing that in the composite fiber PAN lattice spacings are slightly smaller than their value in the control gel spun PAN, may explain the reduced PAN/SWNT solubility.

The stress–strain curve of the highly drawn control PAN fiber shows a yield point at about 25% of the ultimate stress and frequent sudden stress reduction at various strain levels (Fig. 12). These sudden stress reductions were a result of fibril breakage in the highly drawn control PAN fiber and not due to fiber slippage from the grips. The stress–strain curves in Fig. 12 also show that such stress reduction and hence fibril breakage did not occur in the composite fibers. The tensile modulus and strength of the gel spun PAN fiber increased almost linearly up to a draw ratio of about 40, and above this value, draw ratio only had moderate effect on tensile properties (Table 2, Fig. 13). Draw ratio of 51, as well as tensile strength and tensile modulus (Fig. 14) of fully drawn fiber obtained in this study, are consistent with the literature report [22]

Fiber tensile properties are listed in Table 3. With the addition of 1 wt% SWNT, room temperature modulus increased by 6.6 GPa (from 22.1 to 28.7 GPa). Assuming that the PAN modulus in the composite fiber is the same as in the control gel spun PAN, the modulus of the PAN/SWNT composite with fully exfoliated SWNT with an orientation

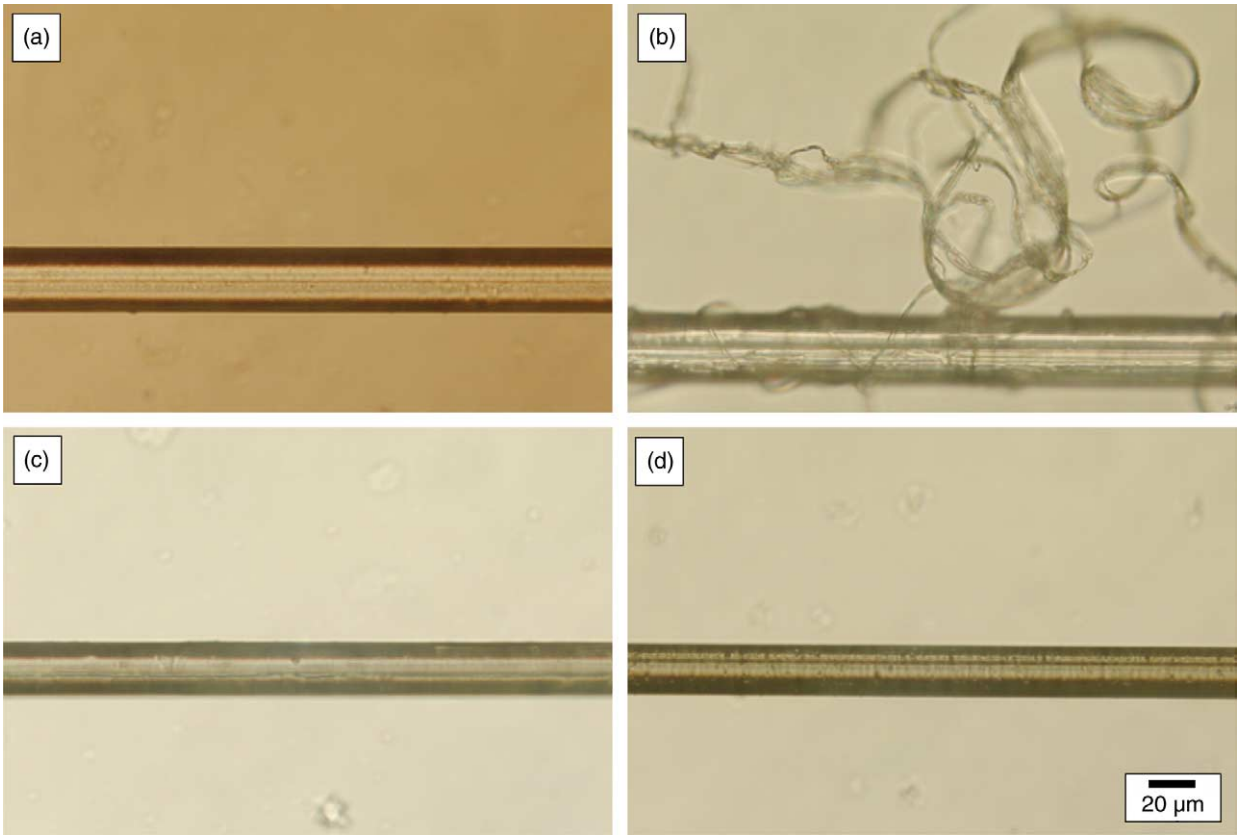

Fig. 11. Optical micrographs of (a) PAN fiber (draw ratio 51) and (c) PAN/SWNT (1 wt%, draw ratio 51), (b) and (d) are the respective fiber after treatment in DMF at 60 °C for 6 h.

factor of 0.915 calculated using previously published method [8,11,24] is plotted in Fig. 15. The composite fiber modulus calculated assuming ideal SWNT orientation, and the observed moduli values are also plotted in this Figure. Observed composite fiber modulus is same as predicted assuming ideal SWNT orientation. However, when the observed SWNT orientation is taken into consideration, then one can see that experimental modulus is higher than the predicted value. This suggests a change in the PAN matrix modulus with the incorporation of SWNTs. This is consistent with the slightly higher PAN crystallinity and orientation in the composite fiber.

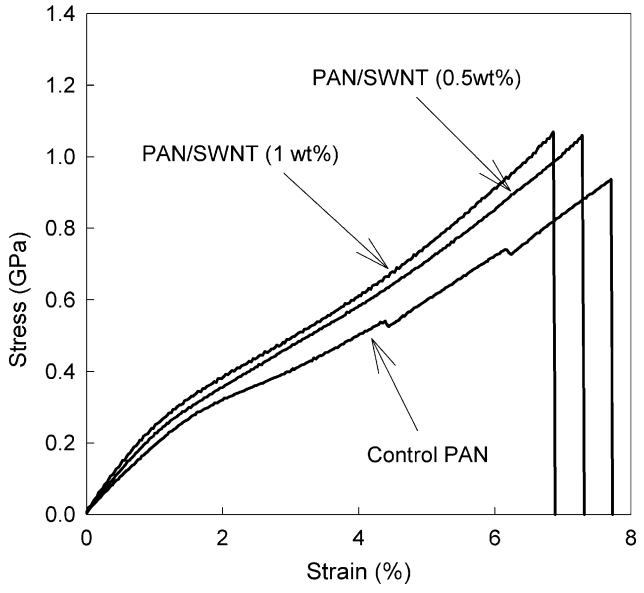

Fig. 12. Typical stress–strain curves for PAN and PAN/SWNT composite fibers.

Tan δ as a function of temperature at a frequency of 10 Hz shows relaxations at ~140, 75, and 25 °C (Fig. 16(a)). These transitions are generally termed as α (and α_c), β_c, and γ, respectively. Despite higher frequency (10 Hz), these transition temperature values are lower than the literature reported values [20] of 150, 100, and 25 °C at 3.5 Hz, respectively. However, it is noted that the molecular weight in this literature reported study is an order of magnitude higher (2.3×10^6 g/mol) than

Table 2
Mechanical properties of gel-spun PAN fiber at various draw ratios

	Draw ratio*				
	22	32	38	45	51
Diameter (μm)	32.4±0.4	27.2±0.4	23.6±0.2	22.1±0.3	20.8±0.2
Tensile modulus (GPa)	14.5±1.3	17.8±1.2	21.0±2.2	21.2±2.5	22.1±1.2
Tensile strength (GPa)	0.58±0.05	0.76±0.08	0.85±0.14	0.88±0.10	0.90±0.18
Strain to failure (%)	8.4±0.9	8.1±1.0	7.9±1.2	7.8±0.8	7.4±0.8
Work of rupture (MPa)	26±5	32±6	35±9	35±7	35±9

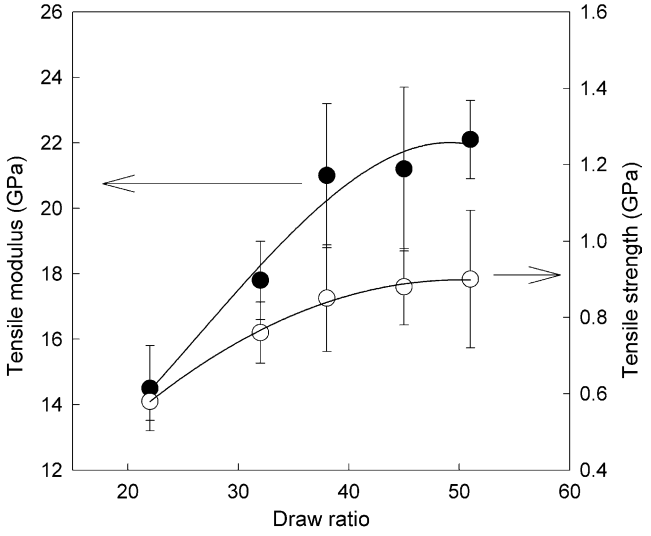

Fig. 13. The tensile modulus and tensile strength of gel-spun PAN fibers as a function of draw ratio.

the molecular weight used in the current study (2.5×10^5 g/mol). The α relaxation was attributed to the micro-Brownian motion in the amorphous phase, which can vanish upon annealing or drawing, and α_c relaxation is likely associated with the molecular motion in syndiotactic or short isotactic sequences. β_c relaxation was reported to exist in both iso- and atactic-PAN, and was attributed to the molecular motion from helical sequences in the paracrystalline regions. The γ relaxation was attributed to the local motion in the syndiotactic or short isotactic sequences (the planar zigzag conformation), and the long tail of γ relaxation down to -150 °C is ascribed to the various local motions for conformationally disordered regions. β_c transition in the composite fiber were of reduced magnitude, broader, and shifted to higher temperature as compared to the control PAN fiber. Since, β_c relaxation is

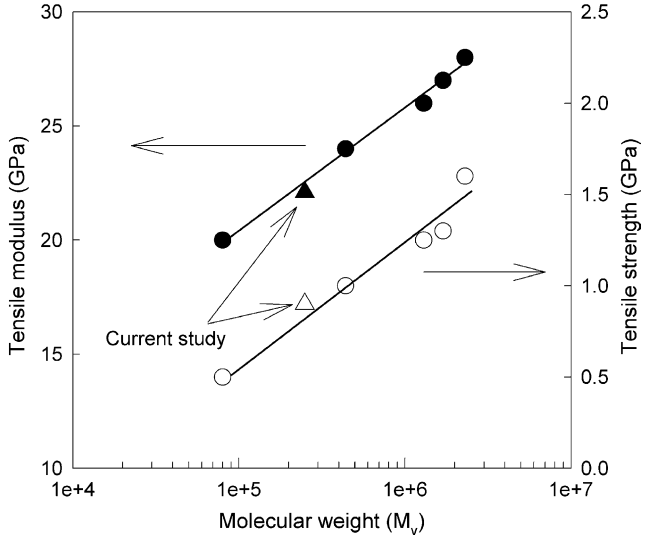

Fig. 14. Tensile modulus and tensile strength of fully drawn atactic-PAN fiber or film as a function of molecular weight. The circles represent the data from Ref. [22] and the triangles are the experimental data from the current study.

Table 3
Mechanical properties of the gel-spun PAN and PAN/SWNT composite fibers (draw ratio = 51)

	Diameter (μm)	Tensile modulus (GPa)	Tensile strength (GPa)	Strain to failure (%)	Work of rupture (MPa)
PAN	20.8±0.2	22.1±1.2	0.90±0.18	7.4±0.8	35±9
PAN/SWNT (0.5 wt%)	19.6±0.3	25.5±0.8	1.06±0.14	7.2±0.6	41±8
PAN/SWNT (1 wt%)	18.7±0.2	28.7±2.7	1.07±0.14	6.8±0.8	39±8

strongly dependent on the helical sequences in PAN crystal, this suggests increased planar zigzag sequences in the composite fiber, consistent with the WAXD data, as discussed earlier. The γ transition and its tail down to -100 °C for the composite fiber was nearly identical to the transition for the control PAN fiber, while the magnitude for the α or α_c transition increased with the incorporation of SWNT and slightly shifted to higher temperature.

Tan δ magnitude of PAN/SWNTs (1 wt%) composite β_c peak decreased and all three transition temperatures increased with increasing frequency (Fig. 16(b)). The activation energy calculated using Arrhenius equation and the β_c peak temperatures at various frequencies (Table 4) show significantly higher energy for the composite fiber as compared to that of the control PAN fiber. This suggests that the presence of SWNTs act as a barrier for this motion.

The storage moduli of composite fibers are higher than that of the control PAN fiber in the entire temperature range (Fig. 17(a)). The difference between the storage moduli of fully drawn PAN/SWNT (1 wt%) and PAN fibers at various frequencies plotted in Fig. 17(b) show that nanotube

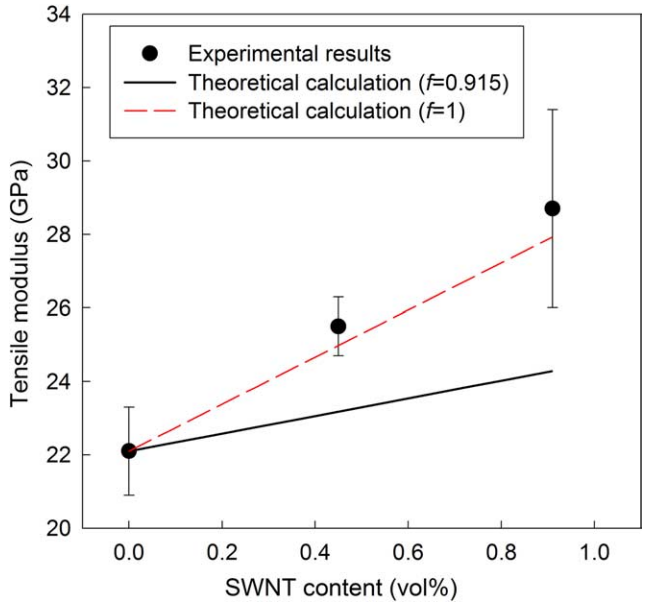

Fig. 15. Tensile modulus of PAN/SWNT fibers (draw ratio 51) as a function of SWNT content. Solid line is the calculated value based on rule of mixtures assuming PAN modulus in the composite is the same as for the control PAN fiber and that the SWNT modulus is 640 GPa. Circles represent the experimental data.

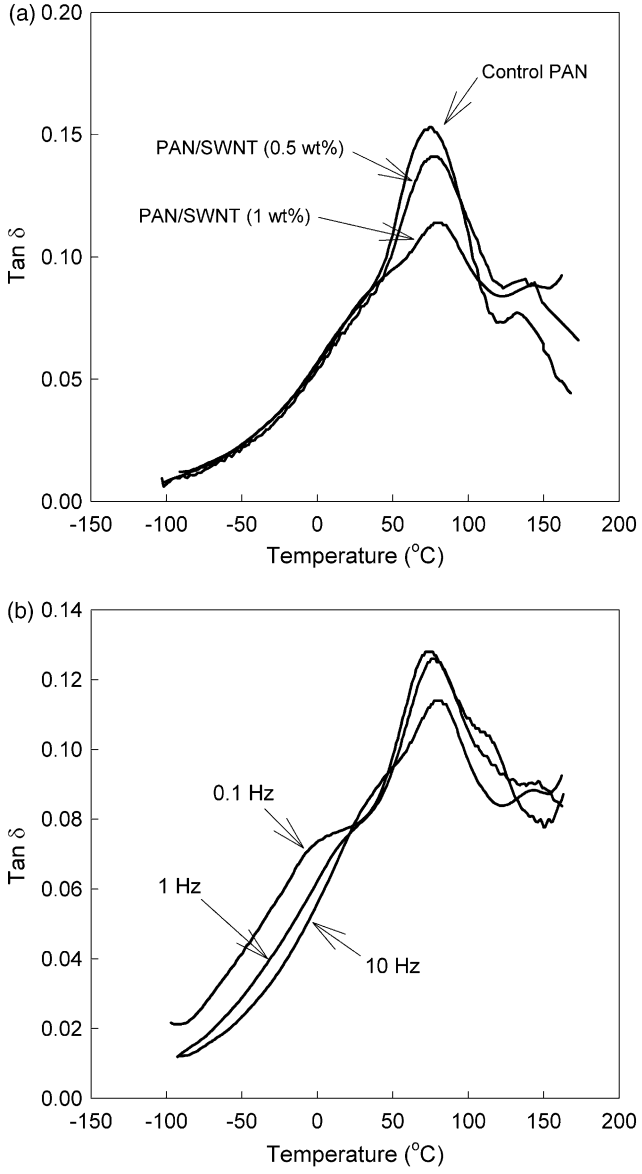

Fig. 16. Tan δ behavior of (a) PAN and PAN/SWNT fibers as a function of temperature at 10 Hz, and (b) PAN/SWNT (1 wt%) fiber at various frequencies. All the specimens were drawn to a draw ratio of 51.

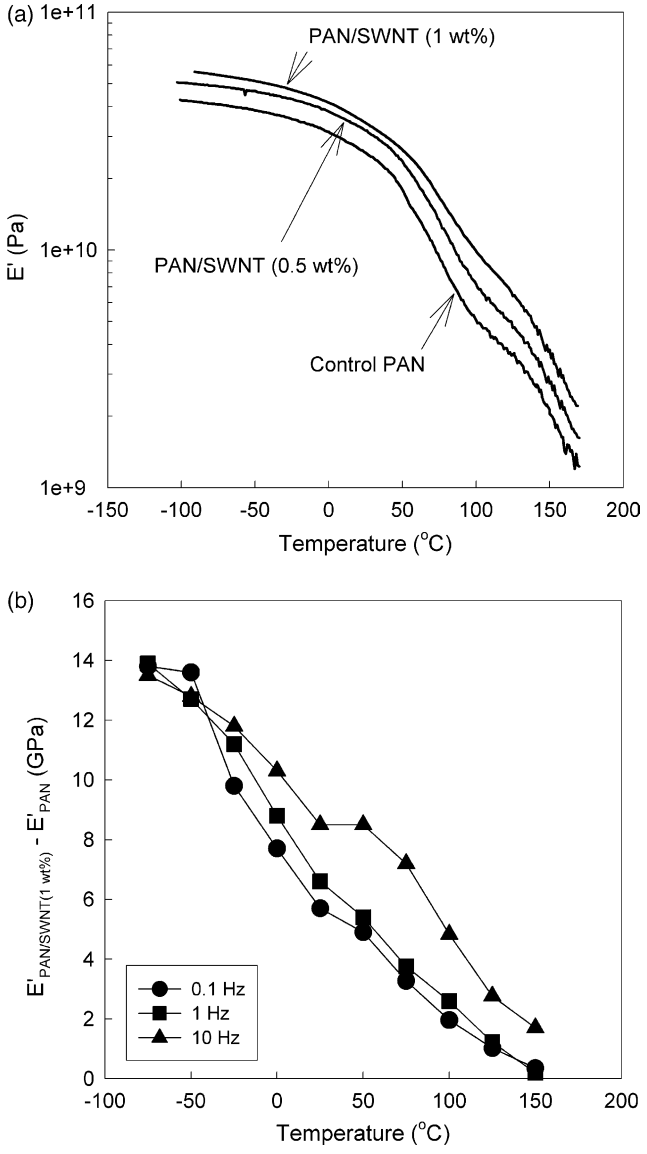

Fig. 17. (a) Storage modulus of PAN and PAN/SWNT fibers as a function of temperature at 10 Hz, and (b) Storage modulus differences between control PAN and PAN/SWNT fibers (1 wt% SWNT) as a function of temperature at various frequencies. All the specimens were drawn to a draw ratio of 51.

Table 4
Dynamic mechanical analysis results for gel spun PAN and PAN/SWNT composite fibers draw ratio = 51)

	β_c Transition temperature (°C) at various frequencies			
	0.1 Hz	1 Hz	10 Hz	E_A (kJ/mol)[a]
Control PAN	66.7	71.1	75	544
PAN/SWNT (0.5 wt%)	71.7	75.1	78	717
PAN/SWNT (1 wt%)	74.6	77.2	80.4	809

The transition temperatures are the tan δ peak temperatures.

[a] E_A is activation energy calculated using Arrhenius equation ($f = A \exp\left(-\frac{E_A}{RT}\right)$, where f, R, and T are frequency, gas constant, and absolute temperature, respectively.

contribution to the storage modulus is decreasing with increasing temperature and increasing with increasing frequency. At −75 °C (198 K), 1 wt% nanotubes contribute ~13.9 GPa to the storage modulus, while this contribution is reduced to 6.6 GPa at 25 °C (298 K), and ~0.2 GPa at 150 °C (423 K) at 1 Hz. Theoretical calculations show that SWNT modulus at 423 K (150 °C) is more than 96% of its value at 0 K [57,58]. Thus, in this temperature range, SWNT modulus is not very sensitive to temperature. Therefore, the strong temperature dependence of the storage modulus contribution arising from SWNT in the gel spun PAN/SWNT composite fiber is unusual and may suggest that load transfer ability and hence interfacial strength is increasing almost monotonically with decreasing temperature, even below the γ transition temperature (~25 °C). Part of the modulus increase may be attributed

to the changes in PAN structure and morphology resulting from the presence of SWNT.

Acknowledgements

This work is supported by the Office of Naval Research (N00014-01-1-0657), Air Force Office of Scientific Research (F49620-03-1-0124 and FA9550-06-1-0122), and Carbon Nanotechnologies, Inc. Polyacrylonitrile was obtained from Exlan Corporation, Japan.

References

[1] Baughman RH, Zakhidov AA, de Heer WA. Science 2002;297:787–92.
[2] Biercuk MJ, Llaguno MC, Radosavljevic M, Hyun JK, Johnson AT, Fischer JE. Appl Phys Lett 2002;80:2767–9.
[3] Kim B, Lee J, Yu IS. J Appl Phys 2003;94:6724–8.
[4] Ko F, Gogotsi Y, Ali A, Naguib N, Ye HH, Yang GL, et al. Adv Mater 2003;15:1161–5.
[5] Kumar S, Dang TD, Arnold FE, Bhattacharyya AR, Min BG, Zhang XF, et al. Macromolecules 2002;35:9039–43.
[6] Sandler JKW, Kirk JE, Kinloch IA, Shaffer MSP, Windle AH. Polymer 2003;44:5893–9.
[7] Shaffer MSP, Windle AH. Adv Mater 1999;11:937–41.
[8] Sreekumar TV, Liu T, Min BG, Guo H, Kumar S, Hauge RH, et al. Adv Mater 2004;16:58–61.
[9] Zhang XF, Liu T, Sreekumar TV, Kumar S, Moore VC, Hauge RH, et al. Nano Lett 2003;3:1285–8.
[10] Putz KW, Mitchell CA, Krishnamoorti R, Green PF. J Polym Sci, Part B: Polym Phys 2004;42:2286–93.
[11] Liu T, Kumar S. Nano Lett 2003;3:647–50.
[12] Chawla KK. Fibrous materials. Cambridge: Cabridge University Press; 1998. 214–219.
[13] Minus ML, Kumar S. JOM 2005;57:52–8.
[14] Smith P, Lemstra PJ. J Polym Sci, Part B: Polym Phys 1981;19:1007–9.
[15] Smith P, Lemstra PJ, Kalb B, Pennings AJ. Polym Bull 1979;1:733–6.
[16] Cha WI, Hyon SH, Ikada Y. J Polym Sci Part B-Polym Phys 1994;32: 297–304.
[17] Takahashi T, Suzuki K, Aoki T, Sakurai K. J Macromol Sci, Phys B 1991; 30:101–18.
[18] Qian BJ, Lin WP, He JM, Hu PP, Wu CX. J Polym Eng 1996;15:327–45.
[19] Sawai D, Kanamoto T, Porter RS. Macromolecules 1998;31:2010–2.
[20] Sawai D, Kanamoto T, Yamazaki H, Hisatani K. Macromolecules 2004; 37:2839–46.
[21] Sawai D, Yamane A, Kameda T, Kanamoto T, Ito M, Yamazaki H, Hisatani K. Macromolecules 1999;32:5622–30.
[22] Sawai D, Yamane A, Takahashi H, Kanamoto T, Ito M, Porter RS. J Polym Sci, Part B: Polym Phys 1998;36:629–40.
[23] Yamane A, Sawai D, Kameda T, Kanamoto T, Ito M, Porter RS. Macromolecules 1997;30:4170–8.
[24] Chae HG, Sreekumar TV, Uchida T, Kumar S. Polymer 2005;46: 10925–35.
[25] Ge JJ, Hou HQ, Li Q, Graham MJ, Greiner A, Reneker DH, et al. J Am Chem Soc 2004;126:15754–61.
[26] Guo H, Sreekumar TV, Liu T, Minus M, Kumar S. Polymer 2005;46: 3001–5.
[27] Kim SH, Min BG, Lee SC, Park SB, Lee TD, Park M, et al. Fiber Polym 2004;5:198–203.
[28] Koganemaru A, Bin Y, Agari Y, Matsuo M. Adv Funct Mater 2004;14: 842–50.
[29] Lam HL, Naguib N, Ye HH, Ali A, Gogotsi Y, Yang GL, et al. Abstracts Papers Am Chem Soc 2003;226:U403–U40U.
[30] Min BG, Sreekumar TV, Uchida T, Kumar S. Carbon 2005;43:599–604.
[31] Oya A, Yokoyama T, Yamamoto M, Hulicova D. Key Eng mater 2004; 264–268:2275–8 [Viii, Pts1–3].
[32] Petrov P, Lou XD, Pagnoulle C, Jerome C, Calberg C, Jerome R. Macromol Rapid Commun 2004;25:987–90.
[33] Pirlot C, Mekhalif Z, Fonseca A, Nagy JB, Demortier G, Delhalle J. Chem Phys Lett 2003;372:595–602.
[34] Pirlot C, Willems I, Fonseca A, Nagy JB, Delhalle J. Adv Eng Mater 2002;4:109–14.
[35] Wang B, Li JW, Wang HP, Jiang JM, Liu YQ. Macromol Symp 2004;216: 189–94.
[36] Weisenberger MC, Grulke EA, Jacques D, Rantell T, Andrews R. J Nanosci Nanotechnol 2003;3:535–9.
[37] Ye HH, Lam H, Titchenal N, Gogotsi Y, Ko F. Appl Phys Lett 2004;85: 1775–7.
[38] Samuels RJ. Structured polymer properties. New York: Wiley; 1974. 28–41.
[39] Allen RA, Ward IM, Bashir Z. Polymer 1994;35:4035–40.
[40] Allen RA, Ward IM, Bashir Z. Polymer 1994;35:2063–71.
[41] Colvin BG, Storr P. Eur Polym J 1974;10:337–40.
[42] Kumamaru F, Kajiyama T, Takayanagi M. J Cryst Growth 1980;48: 202–9.
[43] Bashir Z. J Polym Sci, Part B: Polym Phys 1994;32:1115–28.
[44] Bashir Z. In: Jassal M, Agrawal AK, editors. Order and morphology in atactic polyacrylonitrile, International conference on emerging trends in polymers and textiles. IIT Delhi, India: Deptartment of Textile Technology; 2005. p. 17–28.
[45] Minus M, Chae HG, Kumar S. polymer, in press.
[46] Haggenmueller R, Zhou W, Fischer JE, Winey KI. J Nanosci Nanotechnol 2003;3:105–10.
[47] Potschke P, Brunig H, Janke A, Fischer D, Jehnichen D. Polymer 2005; 46:10355–63.
[48] Zhao Q, Wagner HD. In: Philosophical transactions of the Royal Society of London series a-mathematical physical and engineering sciences, 362; 2004, 2004. p. 2407–24.
[49] Ericson LM, Fan H, Peng HQ, Davis VA, Zhou W, Sulpizio J, et al. Science 2004;305:1447–50.
[50] Li YL, Kinloch IA, Windle AH. Science 2004;304:276–8.
[51] Miaudet P, Badaire S, Maugey M, Derre A, Pichot V, Launois P, et al. Nano Lett 2005;5:2212–5.
[52] Motta M, Li YL, Kinloch I, Windle A. Nano Lett 2005;5:1529–33.
[53] Vigolo B, Penicaud A, Coulon C, Sauder C, Pailler R, Journet C, et al. Science 2000;290:1331–4.
[54] Zhou W, Vavro J, Guthy C, Winey KI, Fischer JE, Ericson LM, et al. J Appl Phys 2004;95:649–55.
[55] Liu T, Kumar S. Chem Phys Lett 2003;378:257–62.
[56] McBrierty VJ, Ward IM. J Phys D: Appl Phys 1968;1:1529–42.
[57] Jiang H, Huang Y, Hwang KC. J Eng Mater Technol-Trans Asme 2005; 127:408–16.
[58] Raravikar NR, Keblinski P, Rao AM, Dresselhaus MS, Schadler LS, Ajayan PM. Phys Rev B 2002;66:235424.